Efficient and Sustained Photoelectrochemical Water Oxidation by Cobalt Oxide/Silicon Photoanodes with Nanotextured Interfaces

Jinhui Yang,[†,‡] Karl Walczak,[†,‡] Eitan Anzenberg,[†,‡] Francesca M. Toma,[†,¶] Guangbi Yuan,[§] Jeffrey Beeman,[†,‡] Adam Schwartzberg,[∥] Yongjing Lin,[†,‡,⊥] Mark Hettick,[†,‡,⊥] Ali Javey,[†,⊥] Joel W. Ager,[†,‡] Junko Yano,[†,§] Heinz Frei,[†,§] and Ian D. Sharp*[,†,§]

[†]Joint Center for Artificial Photosynthesis (JCAP), Lawrence Berkeley National Laboratory, Berkeley, California 94720, United States
[‡]Material Sciences Division, [¶]Chemical Sciences Division, [§]Physical Biosciences Division, and [∥]Molecular Foundry, Lawrence Berkeley National Laboratory, Berkeley, California 94720, United States
[⊥]Electrical Engineering and Computer Sciences, University of California, Berkeley, California 94720, United States

Ⓢ *Supporting Information*

ABSTRACT: Plasma-enhanced atomic layer deposition of cobalt oxide onto nanotextured p^+n-Si devices enables efficient photoelectrochemical water oxidation and effective protection of Si from corrosion at high pH (pH 13.6). A photocurrent density of 17 mA/cm^2 at 1.23 V vs RHE, saturation current density of 30 mA/cm^2, and photovoltage greater than 600 mV were achieved under simulated solar illumination. Sustained photoelectrochemical water oxidation was observed with no detectable degradation after 24 h. Enhanced performance of the nanotextured structure, compared to planar Si, is attributed to a reduced silicon oxide thickness that provides more intimate interfacial contact between the light absorber and catalyst. This work highlights a general approach to improve the performance and stability of Si photoelectrodes by engineering the catalyst/semiconductor interface.

Artificial photosynthesis, by photoelectrochemical splitting of water into H$_2$ and O$_2$, is a promising approach to renewable energy conversion.[1] Critical challenges toward the realization of scalable devices include the availability of suitable semiconductors for capturing the solar spectrum, efficient coupling of catalysts with semiconductors, and stability under aqueous conditions.[2] Furthermore, avoiding explosive product mixtures and reducing efficiency losses due to gas crossover necessitate incorporation of membranes in current integrated systems.[2b,3] In the absence of recirculation, this imposes a requirement for operation under extreme pH conditions in order to eliminate pH gradients.[3] Given the scarcity of acid-stable oxygen evolution reaction (OER) catalysts,[4] the development of efficient and stable photoanodes that operate in alkaline conditions is vital to achieve an efficient solar-to-fuel system.

Silicon is an attractive semiconductor for solar fuel generation since it absorbs a significant fraction of the solar spectrum, is earth-abundant, and is widely used in photovoltaic applications.[5] However, the realization of silicon based solar-to-fuel devices is challenging due to the intrinsic instability of this material under aqueous conditions, particularly at high pH. In recent years, strategies for stabilizing photoanodes against corrosion and

photocorrosion have been widely explored.[1d,6] General approaches involve introducing thin corrosion protection layers that allow interfacial charge transfer of photogenerated minority carriers while physically protecting the light-absorbers. For example, np-Si devices have been passivated with transparent conductive oxides (TCOs) and can function well in near-neutral pH conditions when effectively interfaced with an OER catalyst (Co-Pi).[6c,d] In an alternative approach, Chen et al. showed effective protection of n-Si by atomic layer deposition (ALD) of a 2 nm thick layer of TiO$_2$, followed by e-beam evaporation of Ir as the OER catalyst.[6e] Water oxidation on these protected photoanodes was sustained for >8 h under various pH conditions, including 1 M NaOH, whereas analogous Si photoanodes without TiO$_2$ quickly failed. While incorporation of interfacial corrosion protection layers significantly improves stability by physically separating the photoanode from the electrolyte, such layers can introduce series resistance and recombination losses.[6e] To overcome these limitations, attempts have been made to utilize the OER catalyst itself for protection of Si photoanodes. MnO$_x$ was shown to improve the stability of n-Si in 1 M KOH.[6b] However, corrosion in this harsh alkaline environment limited the operation time to 30 min. Very recently, e-beam evaporation of a thin Ni film on n-Si was used to simultaneously act as both the catalyst and protection layer; long-term stability was shown in the presence of a LiBi-KBi electrolyte at intermediate pH, and up to 24 h stability was achieved in 1 M KOH under 2.2 sun illumination.[1d] This approach requires precise control of ultrathin layers to achieve appreciable photovoltages. In the present work,[7] we show that direct deposition of cobalt oxide (CoO$_x$) by plasma-enhanced ALD on nanotextured p^+n-Si buried junction devices enables effective protection of Si for at least 24 h at high pH (1 M NaOH, pH 13.6), while retaining a high photovoltage (610 mV) under simulated 1 sun irradiation.

Figure 1a shows a schematic illustration of the photoanode preparation processes. First, n-Si (100) wafers were doped with boron using two different methods: drive-in diffusion and ion implantation, followed by etching in buffered HF (see SI). Next, nanotexturing of Si was achieved via Ar plasma sputtering under
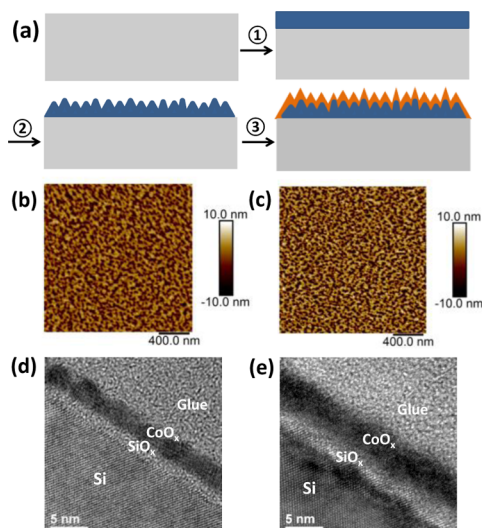
Figure 1. (a) Schematic description of the preparation of nanotextured CoO_x/p^+n-Si device: (1) formation of p^+n-Si by diffusion or implantation of boron into (100) n-Si; (2) nanotexturing by Ar sputtering under substrate bias; (3) CoO_x deposition by ALD. AFM images of the corresponding (b) nanotextured p^+n-Si and (c) nanotextured CoO_x/p^+n-Si reveal rms roughness values of 3.0 and 4.2 nm, respectively. Cross section TEM images of planar (d) and nanotextured (e) structures after CoO_x deposition.

an applied substrate bias, a process that did not impact the open circuit voltage (*vide infra*). The effect of substrate bias sputtering on the morphology of the p^+n-Si surface was studied by atomic force microscopy (AFM) (Figures 1b and S1a). After Ar sputtering, the root-mean-square (rms) surface roughness increased from 1.3 to 3.0 nm (Figures S1a and 1c). Finally, CoO_x was deposited on top of the nanotextured surface by ALD, a process that is uniquely suited for conformal deposition of overlayers on nanostructures due to its self-limiting nature and precise thickness control[8] and has been shown to enhance the stability of metal oxide photoanodes.[9] For comparative studies, CoO_x ALD was also performed on planar p^+n-Si surfaces, as described throughout the text. AFM analysis following catalyst deposition (Figure 1d) reveals a roughness value of 4.2 nm for CoO_x/p^+n-Si with nanotextured interfaces. The increase of surface roughness is consistent with previous reports[8] and is also similar on planar surfaces (increasing from 1.3 to 2.9 nm, Figure S1), confirming that ALD is suitable for conformal CoO_x deposition and retention of the substrate surface texture. Cross-sectional transmission electron micrographs (TEM) (Figures 1d,e and S2) reveal the presence of interfacial silicon oxide layers on both planar and nanotextured samples. While the thickness of this layer is approximately constant for the planar substrate, it varies considerably with position on the nanotextured substrate, with a separation between CoO_x and Si of just a few atomic layers in some regions. Despite identical ALD conditions, CoO_x is found to be polycrystalline when deposited on planar Si but amorphous when deposited on nanotextured surfaces. While the origin of this structural difference is not currently known, it likely plays an important role in the stability of photoelectrodes under alkaline conditions, as discussed below.

The photoelectrochemical current density vs applied potential (*J–E*) characteristics of both planar and nanotextured CoO_x/p^+n-Si were measured in aqueous 1 M NaOH (pH 13.6) under 100 mW/cm² simulated air mass (AM) 1.5 illumination as a function of CoO_x thickness (Figure S3). Consistent with

previous reports, bare Si without a catalyst degraded rapidly.[1d] Likewise, all devices with <1 nm CoO_x layers (<10 cycles) were unstable and exhibited a poor photoresponse.

This is in stark contrast with previous measurements of nanostructured hematite photoanodes,[10] which are inherently stable under alkaline conditions and displayed dramatically improved photocatalytic behavior upon ALD of submonolayer CoO_x. In the present work, introduction of catalytically active surface sites is necessary but not sufficient for effective PEC; thicker CoO_x layers are required to ensure conformal coating and stabilize the surface against corrosion. For all investigated CoO_x thicknesses of 2 nm and above (≥30 ALD cycles), nanotextured devices consistently exhibited a cathodic shift of the open circuit potential and higher current density relative to corresponding planar devices (Figures S3 and S4). Measurements of the incident-photon-to-current-efficiency (IPCE) and dependence of photocurrent on light intensity further confirm the improved performance of nanotextured devices (Figures S5 and S6). The PEC behavior of nanotextured substrates with 100 plasma-enhanced ALD cycles (~4–5 nm) is characterized by a photocurrent density of 17 mA/cm² at thermodynamic OER potential (1.23 V vs RHE) and a saturation current density of 30 mA/cm² (Figure 2a). An identical ALD CoO_x film was applied to
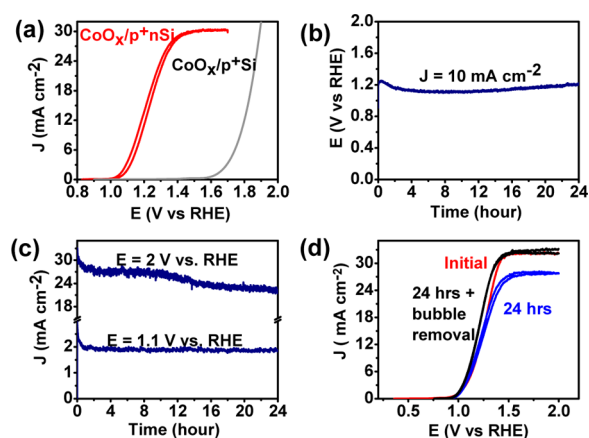
Figure 2. Photoelectrochemical behavior of nanotextured CoO_x/p^+n-Si photoanode in aqueous 1.0 M NaOH under 100 mW/cm² of simulated solar illumination. (a) *J–E* response of CoO_x/p^+n-Si (red) under illumination and CoO_x/p^+ Si (gray) in the dark. (b) Chronopotentiometry of nanotextured CoO_x/p^+n-Si photoanode at a constant current density of 10 mA/cm². (c) Chronoamperometry of nanotextured CoO_x/p^+n-Si photoanode at 2 and 1.1 V vs RHE. (d) *J–E* response of nanotextured photoanodes before (red) and immediately after (blue) 24 h *J–t* stability testing. Clearing of bubbles results in complete recovery of the original *J–E* characteristic (black).

a p^+-Si wafer (0.001–0.005 Ω cm), which provides the baseline performance of the OER electrocatalyst. This measurement reveals that the photovoltage generated with the ion implanted p^+n-Si junction is 610 mV. This value is in good agreement with modern p^+-emitter/n-base single crystalline Si photovoltaics[11] and confirms that the physical nanotexturing process, together with a subsequent etching and catalyst deposition process, does not introduce deleterious near-surface recombination centers.

In order to elucidate the superior photoelectrochemical *J–E* performance for the nanotextured CoO_x/p^+n-Si device, cyclic voltammetry in the presence of a benchmark electrolyte composed of a ferri/ferrocyanide aqueous solution[6e] was performed and compared to the planar device. The peak-to-

peak splitting was 0.25 V on the nanotextured sample vs 1.2 V on the planar sample (Figure S7). This indicates a substantial decrease of interfacial charge transfer resistance by nanotexturing the interface, which may be attributed to improved tunneling probability across regions of reduced interfacial silicon oxide thickness compared to planar systems (Figures 1e and S2).

Photoelectrode stability is an essential requirement and outstanding challenge for solar-to-fuel devices.[2a,b] In the present work, stability was assessed via both chronopotentiometric ($V-t$) and chronoamperometric ($J-t$) operation of CoO_x/p^+n-Si devices. As shown in Figure 2b, $V-t$ curves at a constant current density of 10 mA/cm^2, which is the approximate operational current density expected for overall solar-to-fuel conversion devices achieving 10% efficiency,[2a,4] reveal that nanotextured CoO_x/p^+n-Si devices maintain stable activity for at least 24 h in 1 M NaOH. $J-t$ evaluation (Figure 2c) further confirms the stability of nanotextured CoO_x/p^+n-Si. Stability measurements were performed under conditions of photocurrent saturation, as well as near the open circuit potential, where the current density is particularly sensitive to degradation. Bubble accumulation during testing leads to some reduction of the photocurrent density. However, as shown in Figure 2d, clearing of bubbles results in complete recovery of the original $J-E$ characteristic, proving the stability of nanotextured CoO_x/p^+n-Si over 24 h of continuous operation of under alkaline conditions. In contrast, the planar device is characterized by a decrease of photocurrent during the first 30 min of operation (Figures S8 and S9). XPS analysis reveals that there is no loss of Co from the nanotextured surface following testing for 24 h in 1 M NaOH (Figure S10). These results highlight the stability enhancement provided by ALD of CoO_x onto nanotextured Si devices.

Further insights into the stability of nanotextured photo-anodes was obtained by X-ray fluorescence mapping (XRF) after chronoamperometric testing and by comparison to planar photoanodes. For XRF measurements, a portion of the electrode surface was masked to prevent electrolyte contact with the surface of the electrode. Figure 3a, b show Co $K\alpha$ XRF across the masked edge. In the case of the planar structure, an average of 10% loss of Co from the surface after 1 h stability test is observed (Figure 3a). In contrast, no loss of catalyst is observed from the nanotextured device (Figure 3b). Complementary AFM measurements of electrodes after the PEC stability test provide further information about corrosion processes. While the surface morphology of the nanotextured device is unaffected by prolonged operation under OER conditions, there is substantial corrosion on the planar surfaces, as evidenced by significant morphological changes after 1 h (Figure 3c, d) and 24 h (Figure S11). Together, these XRF and AFM measurements indicate that, in the case of planar devices, etching of the underlying Si occurs under strongly alkaline conditions. In contrast, nano-texturing enhances catalyst durability on the surface, thereby stabilizing the device against corrosion.

In addition to stability under OER conditions, where anodic passivation of Si by silicon oxide could mask certain corrosion mechanisms, it is important for photoelectrodes to exhibit long-term stability under unbiased dark conditions (i.e., at night). Therefore, chemical stability of CoO_x/p^+n-Si was also studied by soaking the electrodes in 1 M NaOH for 24 h. Comparison of AFM images shows no obvious morphological changes to the nanotextured sample, while significant corrosion is observed on the planar sample (Figure S12). Furthermore, XPS analysis reveals no loss of CoO_x from the nanotextured electrode (Figure S13). Importantly, XPS also indicates that no CoO_x is lost from the surface of planar material upon unbiased soaking (Figure S13), despite under-etching of the Si substrate. These results suggest that CoO_x is chemically stable in the alkaline environment, though CoO_x is lost from planar surfaces under OER conditions (Figure 3a), likely as a consequence of simultaneous etching of Si and bubble formation. These results, combined with TEM, point to a possible mechanism for the enhanced stability of nanotextured compared to planar electrodes. We hypothesize that the amorphous nature of the catalyst on nanotextured surfaces is highly conformal due to the lack of crystallites, thereby preventing attack of the substrate by the alkaline solution. In contrast, polycrystalline material may be associated with higher pinhole densities in intergrain regions that permit contact of the electrolyte with the substrate. Additional experiments are underway to test this hypothesis.

Previous reports of CoO_x ALD on a variety of substrates have found different chemical compositions including Co(II), as either CoO or Co(OH)$_2$, and Co$_3$O$_4$.[8−10,12] In the present work, the surface composition of as-deposited films as a function of thickness was investigated using XPS (Figure S14). Following 10 ALD cycles, the Co $2p_{3/2}$ peak exhibits a strong satellite feature at 786.3 eV that is indicative of a film dominated by Co(II). As the film thickness increases, the relative intensity of this satellite feature decreases, the primary Co $2p_{3/2}$ emission line shifts to lower binding energies, and a satellite feature near 789.6 eV emerges. These changes indicate that the surfaces of thicker CoO_x films are dominated by Co$_3$O$_4$, as confirmed by comparison to reference spectra (Figure S15), as well as existing literature.[13]

Since XPS is only sensitive to surface composition, X-ray absorption near-edge spectroscopy (XANES) was used for complementary analysis of the overall composition of ALD thin films. XANES data collected following 60 ALD cycles, together with Co$_3$O$_4$ and Co(OH)$_2$ reference spectra, are shown in Figure 4b. Fitting a linear combination of the reference spectra to data from the ALD CoO_x revealed that the thin films are composed of ∼20% Co(II) and ∼80% of Co$_3$O$_4$, whereas XPS indicated that the surface is dominated by Co$_3$O$_4$. These combined results indicate that the thick ALD CoO_x films are composed of Co$_3$O$_4$ with an underlying interfacial Co(II), most likely CoO, considering the Co(Cp)$_2$ precursor and O$_2$ plasma used in
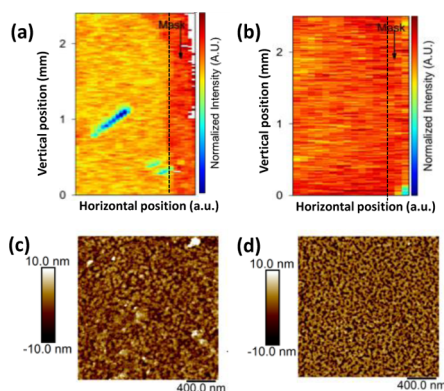
Figure 3. X-ray fluorescence (XRF) mapping with an excitation energy of 8409 eV across the edge (vertical line) of masked and exposed areas of (a) planar and (b) nanotextured CoO_x/p^+n-Si after chronoampero-metric testing for 1 h. AFM of (c) planar and (d) nanotextured CoO_x/p^+n-Si after photoanodic operation. The former exhibits significant corrosion, while the latter retains its initial morphology and homogeneity.
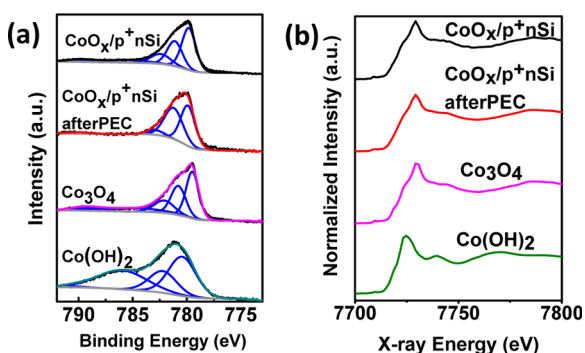
Figure 4. (a) XPS (Co $2p_{3/2}$) and (b) XANES (Co K-edge) spectra of CoO_x/p^+n-Si samples: as-deposited and after PEC stability testing for 1 h at an overpotential of 400 mV in 1 M NaOH (pH 13.6), as well as Co_3O_4 and $Co(OH)_2$ standards.

deposition. The composition following PEC testing for 1 hour was also examined by XPS and XANES. While XANES reveals that the bulk of the film is composed of a fixed ratio of Co_3O_4 and $Co(OH)_2$ (Figure 4b), XPS shows transformation of the surface to CoO(OH) (Figures 4a, S16 and S17), which is in consistent with previous reports.[14] We note that the same composition behavior is observed on both planar and nanotextured Si surfaces, despite the different structures of these films.

In conclusion, we have developed a straightforward approach to dramatically improve the activity and stability of Si photoanodes by plasma-enhanced ALD on nanotextured Si surfaces formed via physical Ar sputtering of p^+n-Si devices. Photovoltages as high as 610 mV were obtained, with stable operation for at least 24 h in 1 M NaOH under simulated solar illumination. Nanotexturing the interface between CoO_x and Si decreases interfacial charge transfer resistance by locally reducing the silicon oxide thickness and increases stability, enabling sustained operation. This work highlights an approach to stabilizing semiconductor photoelectrodes for efficient operation under the harsh conditions required for solar water splitting by engineering catalyst/semiconductor interfaces.

■ ASSOCIATED CONTENT

Ⓢ Supporting Information
Materials, instruments, synthesis, XPS spectra, XANES data, cyclic voltammetry. This material is available free of charge via the Internet at http://pubs.acs.org.

■ AUTHOR INFORMATION

Corresponding Author
idsharp@lbl.gov

Notes
The authors declare no competing financial interest.

■ ACKNOWLEDGMENTS

■ REFERENCES

(1) (a) Lewis, N. S.; Nocera, D. G. *Proc. Natl. Acad. Sci. U.S.A.* **2006**, *103*, 15729. (b) Maeda, K.; Teramura, K.; Lu, D. L.; Takata, T.; Saito, N.; Inoue, Y.; Domen, K. *Nature* **2006**, *440*, 295. (c) Reece, S. Y.; Hamel, J. A.; Sung, K.; Jarvi, T. D.; Esswein, A. J.; Pijpers, J. J. H.; Nocera, D. G. *Science* **2011**, *334*, 645. (d) Kenney, M. J.; Gong, M.; Li, Y.; Wu, J. Z.; Feng, J.; Lanza, M.; Dai, H. *Science* **2013**, *342*, 836. (e) Youngblood, W. J.; Lee, S.-H. A.; Maeda, K.; Mallouk, T. E. *Acc. Chem. Res.* **2009**, *42*, 1966. (f) Dahl, S.; Chorkendorff, I. *Nat. Mater.* **2012**, *11*, 100.

(2) (a) Parkinson, B. *Acc. Chem. Res.* **1984**, *17*, 431. (b) McKone, J. R.; Lewis, N. S.; Gray, H. B. *Chem. Mater.* **2013**, *26*, 407. (c) Yang, J.; Wang, D.; Han, H.; Li, C. *Acc. Chem. Res.* **2013**, *46*, 1900.

(3) Modestino, M. A.; Walczak, K. A.; Berger, A.; Evans, C. M.; Haussener, S.; Koval, C.; Newman, J. S.; Ager, J. W.; Segalman, R. A. *Energy Environ. Sci.* **2014**, *7*, 297.

(4) McCrory, C. C. L.; Jung, S.; Peters, J. C.; Jaramillo, T. F. *J. Am. Chem. Soc.* **2013**, *135*, 16977.

(5) (a) Yuan, G.; Zhao, H.; Liu, X.; Hasanali, Z. S.; Zou, Y.; Levine, A.; Wang, D. *Angew. Chem. In. Ed.* **2009**, *121*, 9860. (b) Boettcher, S. W.; Spurgeon, J. M.; Putnam, M. C.; Warren, E. L.; Turner-Evans, D. B.; Kelzenberg, M. D.; Maiolo, J. R.; Atwater, H. A.; Lewis, N. S. *Science* **2010**, *327*, 185.

(6) (a) Sun, K.; Pang, X.; Shen, S.; Qian, X.; Cheung, J. S.; Wang, D. *Nano Lett.* **2013**, *13*, 2064. (b) Strandwitz, N. C.; Comstock, D. J.; Grimm, R. L.; Nichols-Nielander, A. C.; Elam, J.; Lewis, N. S. *J. Phys. Chem. C* **2013**, *117*, 4931. (c) Cox, C. R.; Winkler, M. T.; Pijpers, J. J. H.; Buonassisi, T.; Nocera, D. G. *Energy Environ. Sci.* **2013**, *6*, 532. (d) Pijpers, J. J.; Winkler, M. T.; Surendranath, Y.; Buonassisi, T.; Nocera, D. G. *Proc. Natl. Acad. Sci. U.S.A.* **2011**, *108*, 10056. (e) Chen, Y. W.; Prange, J. D.; Dühnen, S.; Park, Y.; Gunji, M.; Chidsey, C. E.; McIntyre, P. C. *Nat. Mater.* **2011**, *10*, 539. (f) Contractor, A. Q.; Bockris, J. O. M. *Electrochim. Acta* **1984**, *29*, 1427. (g) Fan, F. R. F.; Keil, R. G.; Bard, A. J. *J. Am. Chem. Soc.* **1983**, *105*, 220. (i) Campet, G.; Puprichitkun, C.; Sun, Z. W. *J. Electroanal. Chem. Interfacial Electrochem.* **1989**, *269*, 435.

(7) This work is part of a focused approach, involving multiple JCAP projects and investigators, dedicated to the protection of otherwise unstable photoelectrodes in aqueous environments.

(8) Donders, M.; Knoops, H.; Kessels, W.; Notten, P. *J. Electrochem. Soc.* **2011**, *158*, G92.

(9) Lichterman, M. F.; Shaner, M. R.; Handler, S. G.; Brunschwig, B. S.; Gray, H. B.; Lewis, N. S.; Spurgeon, J. M. *J. Phys. Chem. L* **2013**, *4*, 4188.

(10) Riha, S. C.; Klahr, B. M.; Tyo, E. C.; Seifert, S.; Vajda, S.; Pellin, M. J.; Hamann, T. W.; Martinson, A. B. F. *ACS Nano* **2013**, *7*, 2396.

(11) Meier, D. L.; Chandrasekaran, V.; Davis, H. P.; Payne, A. M.; Xiaoyan, W.; Yelundur, V.; O'Neill, E.; Young-Woo, O.; Zimbardi, F.; Rohatgi, A. *IEEE J. Photovolt.* **2011**, *1*, 123.

(12) Diskus, M.; Nilsen, O.; Fjellvåg, H. *Chem. Vap. Deposition* **2011**, *17*, 135.

(13) (a) Biesinger, M. C.; Payne, B. P.; Grosvenor, A. P.; Lau, L. W. M.; Gerson, A. R.; Smart, R. S. C. *Appl. Surf. Sci.* **2011**, *257*, 2717. (b) Yang, J.; Liu, H.; Martens, W. N.; Frost, R. L. *J. Phys. Chem. C* **2009**, *114*, 111.

(14) Kanan, M. W.; Yano, J.; Surendranath, Y.; Dinca, M.; Yachandra, V. K.; Nocera, D. G. *J. Am. Chem. Soc.* **2010**, *132*, 13692.